Detection and characterization of two VLM binaries: LP 1033-31 and LP 877-72

Subhajeet Karmakar, A. S. Rajpurohit, F. Allard, D. Homeier

Monthly Notices of the ROYAL ASTRONOMICAL SOCIETY

MNRAS **498,** 737–749 (2020)
Advance Access publication 2020 July 29

doi:10.1093/mnras/staa2173

Detection and characterization of two VLM binaries: LP 1033-31 and LP 877-72

Subhajeet Karmakar [1]★ A. S. Rajpurohit,[1] F. Allard[2] and D. Homeier[3]

[1]*Astronomy & Astrophysics Division, Physical Research Laboratory, Navrangapura, Ahmedabad 380009, India*
[2]*Univ Lyon, Ens de Lyon, Univ Lyon1, CNRS, Centre de Recherche Astrophysique de Lyon UMR5574, F-69007, Lyon, France*
[3]*Zentrum für Astronomie der Universität Heidelberg, Landessternwarte, Königstuhl 12, D-69117 Heidelberg, Germany*

Accepted 2020 July 22. Received 2020 July 22; in original form 2019 November 30

ABSTRACT

Using the high-resolution near-infrared adaptive optics imaging from the NaCo instrument at the Very Large Telescope, we report the discovery of a new binary companion to the M-dwarf LP 1033-31 and also confirm the binarity of LP 877-72. We have characterized both the stellar systems and estimated the properties of their individual components. We have found that LP 1033-31 AB with the spectral type of M4.5+M4.5 has a projected separation of 6.7 ± 1.3 AU. Whereas with the spectral type of M1+M4, the projected separation of LP 877-72 AB is estimated to be 45.8 ± 0.3 AU. The binary companions of LP 1033-31 AB are found to have similar masses, radii, effective temperatures, and log g with the estimated values of 0.20 ± 0.04 $M_{\odot}$, 0.22 ± 0.03 $R_{\odot}$, and 3200 K, 5.06 ± 0.04. However, the primary of LP 877-72 AB is found to be twice as massive as the secondary with the derived mass of 0.520 ± 0.006 $M_{\odot}$. The radius and log g for the primary of LP 877-72 AB are found to be 1.8 and 0.95 times that of the secondary component with the estimated values of 0.492 ± 0.011 $R_{\odot}$ and 4.768 ± 0.005, respectively. With an effective temperature of 3750 ± 15 K, the primary of LP 877-72 AB is also estimated to be ∼400 K hotter than the secondary component. We have also estimated the orbital period of LP 1033-31 and LP 877-72 to be ∼28 and ∼349 yr, respectively. The binding energies for both systems are found to be $>10^{43}$ erg, which signifies that both systems are stable.

Key words: stars: low-mass – atmospheres – imaging – late-type – fundamental parameters – binaries: general.

1 INTRODUCTION

Most of the stars in the galactic stellar population consist of low-mass stars (Bochanski et al. 2010). These stars show a high level of magnetic activities due to their thick convective envelope above a radiative interior (Pandey & Karmakar 2015; Savanov et al. 2016; Karmakar et al. 2016, 2017). Among these stars, M-dwarfs are the most abundant inhabitants of our Galaxy. These stars also account for over 70 per cent of stellar systems in the solar neighbourhood (Henry et al. 1997). Further, M-dwarfs are the most numerous potential planet hosts of all the stellar classes (Lada 2006). The typical mass of the very low mass (VLM) stars or M-dwarfs ranges from 0.6 $M_{\odot}$ to the hydrogen-burning limit of about 0.075 $M_{\odot}$ (Baraffe et al. 1998). In this paper, the 'VLM binaries' are used to denote the binary systems that consist of VLM+VLM stellar companions.

From the past few decades, following the first discoveries by Nakajima et al. (1995) and Rebolo, Zapatero Osorio & Martín (1995), thousands of VLM stars have been discovered till date. These stars are intrinsically faint due to their small size and low temperature. However, with the advent of large infrared arrays, the number of VLM binaries that have been detected has increased substantially in recent years. Various ground-based surveys such as Sloan Digital Sky Survey (SDSS; York et al. 2000), Two Micron All Sky Survey (2MASS; Cutri et al. 2003; Skrutskie et al. 2006), and space-based surveys such as Wide-field Infrared Survey Explorer (WISE; Wright et al. 2010) have made such discoveries. However, despite the large assemblage of these cool objects, their formation mechanism still remains an open question (e.g. Burgasser et al. 2007b; Luhman et al. 2007; Whitworth et al. 2007; Luhman 2012; Chabrier et al. 2014). In order to explain their origins, various scenarios such as ejection from multiple prestellar cores (e.g. Reipurth & Clarke 2001), turbulent fragmentation of gas in protostellar clouds (e.g. Padoan & Nordlund 2004), photoionizing radiation from massive nearby stars (e.g. Whitworth & Zinnecker 2004), and fragmentation of unstable prestellar discs (e.g. Stamatellos & Whitworth 2009) have been proposed.

The observational studies of VLM binaries can provide effective diagnostics for testing the VLM formation scenarios. This is due to the fact that the formation mechanisms leave their own traces on the statistical properties of binaries such as frequency, orbit separation, and mass-ratio distributions (e.g. Bate 2009). In addition, VLM binaries can provide a model-independent way to determine physical properties, including masses and radii (see Delfosse et al. 2000; Lane, Boden & Kulkarni 2001; Ségransan et al. 2003; Bouy et al. 2004; Konopacky et al. 2010; Dupuy & Liu 2017; Winters et al. 2019b, a). This is fundamental to the calibration of the mass-luminosity relation (Henry & McCarthy 1993; Henry et al. 1999; Ségransan et al. 2000). Hence, for the comprehensive study of the formation scenarios, it is essential to obtain unbiased VLM binary samples from various detection methods that are effective with respect to a different population of VLM objects.

The small size of VLMs makes them suitable candidates to detect planets around them in the habitable zone. Recent studies by Bonfils

★ E-mail: subhajeet09@gmail.com

et al. (2012), Anglada-Escudé et al. (2016), and Gillon et al. (2017) show that M-dwarfs host exoplanets. Recently, few large exoplanet surveys have been started to monitor sizeable numbers of M-dwarfs, such as the M2K programme which is targeting some 1600 M-dwarfs for radial velocity (RV) monitoring (Apps et al. 2010), the CARMENES search for exoplanets around 324 M-dwarfs (Reiners et al. 2018), and the MEarth project (Irwin et al. 2015), which is designed to detect exoplanet transits in nearby late-type M-dwarfs. Among these studies, the brightest M-dwarfs are the ideal (highest priority) targets for high-precision RV searches, whereas the latest M-dwarfs are the most suitable for transit surveys, and the youngest M-dwarfs are preferable targets for adaptive optics (AO) imaging. In the case of VLM binaries, the presence of the companion to the primary star is also very important as they influence planet formation. However, due to limited detection of exoplanetary systems in the binary or multiple systems particularly on VLM stellar systems, the studies of the effect of stellar multiplicity on the planet formation is still statistically insignificant. For example, in case of the stellar systems in the solar neighbourhood, Wang et al. (2014) have shown that compared to the single-star systems, planets in multiple-star systems occur 4.5 ± 3.2, 2.6 ± 1.0, and 1.7 ± 0.5 times less frequently when a stellar companion is present at a distance of 10, 100, and 1000 AU, respectively. Therefore, further observations of the VLM binaries are essential.

The high spatial resolution imaging surveys in recent years enable us to estimate the binary separation for VLM stars. Several studies regarding the binary separation in the last few decades show significant progress. Phan-Bao et al. (2005) have summarized that the binary frequency in the separation range of 1–15 AU is about 15 per cent, whereas the frequency of wide binary systems (semimajor axis >15 AU) is very low, <1 per cent. Moreover, the mass ratios were strongly biased towards nearly equal mass binaries. Other studies showed that from a statistical sample with separation over 3 AU, the typical binary separation was found to be $\sim$4 AU (e.g. Close et al. 2003; Burgasser et al. 2007a; Kraus et al. 2012). Via statistical investigation utilizing a Bayesian algorithm, Allen et al. (2012) found that only 2.3 per cent of VLM objects have a companion in the 40–1000 AU range. Also, Baron et al. (2015) reported the discovery of 14 VLM binary systems with separations of 250–7500 AU. The studies of Gálvez-Ortiz et al. (2017) reported the identification of 36 low and VLM candidates to binary/multiple systems with separations between 200 and 92 000 AU. Recently, Winters et al. (2019a) have derived the projected linear separation distribution of the companions for lower mass primaries to be in the range of 4–20 AU. These differences can be due either to a continuous formation mass-dependent trend or to differences in the formation mechanism of the VLM objects.

Since the proper motion (PM) of a star is inversely proportional to its distance from the observer, a high proper motion (HPM) is a strong selection criterion for proximity. The first attempts at large surveys for HPM stars began in the early 20th century with works by van Maanen (1915), Wolf (1919), and Ross (1939). Later, additional surveys were completed: e.g. Giclas, Burnham & Thomas (1971) and Giclas, Burnham & Thomas (1978). The first all-sky search for nearby stars was carried out by Luyten, who published two PM catalogues: the Luyten Half-Second catalogue (Luyten 1979a) and the New Luyten Two-Tenths catalogue (NLTT; Luyten 1979b, 1980). Luyten's catalogues represent the results of a huge effort over more than three decades and are mainly based on observations with the Palomar Schmidt telescope and the blinking technique applied to pairs of plates with approximately 15 yr of epoch difference. After these early works, many studies on PM have been carried out with different galactic latitude, source magnitude, and PM range (Lépine & Shara 2005; Lépine 2008; Boyd et al. 2011; Lépine & Gaidos 2011; Frith et al. 2013; Lépine et al. 2013; Lépine & Gaidos 2013; Kirkpatrick et al. 2014; Luhman 2014; Smith et al. 2014; Kurtev et al. 2017).

In this paper, we report near-infrared (NIR) detection of VLM companions to two M-dwarfs, LP 1033-31 and LP 877-72, using direct imaging and characterized them. We have discovered that LP 1033-31 is a binary system instead of a 'single' object as known previously. We have also confirmed the binarity of LP 877-72 after the *Gaia* detection of the companion (Gaia Collaboration 2018). Both the objects are far from the galactic plane, and they were first detected as part of HPM surveys (Giclas et al. 1978; Luyten 1995). Later, these objects were also observed as the part of several high proper-motion surveys (Wroblewski & Torres 1995; Pokorny, Jones & Hambly 2003; Salim & Gould 2003; Reylé & Robin 2004; Kirkpatrick et al. 2016; Schneider et al. 2016) The latest estimated values for PM of the systems are $0''.299$ and $0''.305$ per year for LP 1033-31 and LP 877-72, respectively (Muirhead et al. 2018; Stassun et al. 2019). Both of these objects were also studied as a part of the bright M-dwarfs (Lépine & Gaidos 2011; Frith et al. 2013), as well as the solar neighbourhoods (Finch et al. 2014; Winters et al. 2015).

Several investigations of the stellar parameters of LP 1033-31 and LP 877-72 have been performed over the last few decades. The first spectroscopic observations for LP 1033-31 and LP 877-72 as 'single' objects have been performed by Reylé et al. (2006) and Scholz, Meusinger & Jahreiß (2005), respectively. Using visual comparison with the spectral templates as well as from the classification scheme based on the TiO and CaH band strengths, Reylé et al. (2006) derived the spectral for LP 1033-31 to be M3.5. Using the same method, Scholz et al. (2005) derived the spectral type for LP 877-72 to be M3.0. Rajpurohit et al. (2013) had performed the spectral synthesis analysis to determine their atmospheric properties and their fundamental parameters such as $T_{\rm eff}$ and log g by assuming the solar metallicity. The derived $T_{\rm eff}$, spectral type, and log g were found to be equal for both LP 1033-31 and LP 877-72 with the values of 3200 K, M4, and 5.0. Later observations of these parameters show good agreement with these values (Stassun et al. 2018, 2019; Anders et al. 2019). Using TESS data, as 'single' object the mass and radius of LP 1033-31 have been derived as 0.316 $M_{\odot}$ and 0.319 $R_{\odot}$ (Stassun et al. 2019), whereas for LP 877-72, these same parameters have been derived as 0.651 $M_{\odot}$ and 0.556 $R_{\odot}$ (Anders et al. 2019; Stassun et al. 2019). Moreover, in the case of LP 877-72, Gaidos et al. (2014) have discussed the possibility of hosting exoplanets and life. In this work, we have adopted the distance of LP 877-72 derived from the parallax measurement from *Gaia* DR2 to be 33.77 ± 0.17 pc (Bailer-Jones et al. 2018). However, in the case of LP 1033-31, the *Gaia* parallax measurement is not available. Therefore, we have used the latest photometric distance of LP 1033-31 as 16.57 ± 3.27 pc (Finch et al. 2014). Although *Gaia* observations have already detected both the components of LP 877-72, the detailed study of both the components was not previously carried out. Therefore, in this study, we discovered the companion of LP 1033-31 using the high-resolution images. Further, we have characterized both the systems and derived the physical parameters of the identified components.

The paper is organized as follows. The observations are described in Section 2. In Section 3, we discuss the data reduction procedures and ascertain the binary separation, flux ratio, and position angles (PAs). In Sections 4.1 and 4.2, we have derived the NIR magnitudes and spectral classes of the newly discovered stellar components. In Section 5, we describe the other derived system parameters such as mass, radius, and orbital period. In Section 6, we discuss our results and finally in Section 7, we summarized our work.

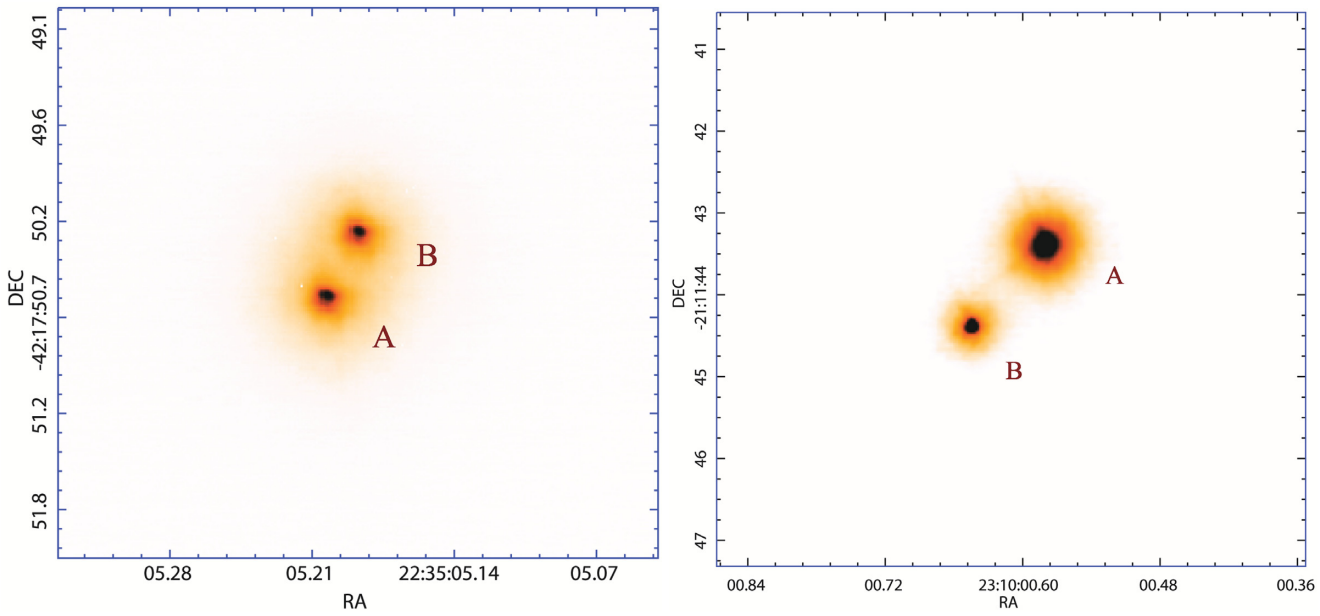

(a) LP 1033-31 (b) LP 877-72

Figure 1. NaCo *J*-band images of (a) LP 1033-31 and (b) LP 877-72. The standard convention is used, i.e. north is up, and east is left. A and B denote the primary and secondary components of both the VLM binaries.

2 OBSERVATIONS

Using the Very Large Telescope (VLT) of European Southern Observatory (ESO, Chile) specifically the Nasmyth Adaptive Optics System (NAOS) and Near-Infrared Imager and Spectrograph (CONICA), popularly known as NaCo (Lenzen et al. 2003; Rousset et al. 2003), two M-dwarfs LP 1033-31 and LP 877-72 were observed under programme ID 091.C-0501(B). A total of 20 frames were observed in each of the JHK_s photometric bands for LP 1033-31 on 2013 July 2. On the same night, LP 877-72 was also observed for 30 frames in each of the JHK_s photometric bands. The exposure time for individual frames was of 30 s. In order to allow an efficient reduction of the sky background, each image was jittered using a jitter box of 5″. Since no bright AO source was available nearby, N90C10 dichroic was used where 90 per cent of the light was utilised for AO and only 10 per cent for the science camera. All the observations for LP 1033-31 were obtained within an airmass range of 1.049–1.051, whereas LP 877-72 were observed within the airmass ranging from 1.002 to 1.010. The seeing condition for the day of observation was also very good ($< 0.85''$). S13 camera was used with a field of view of $14'' \times 14''$ and a pixel scale of 13.2 mas per pixel.

3 DATA REDUCTION AND ANALYSIS

To carry out our analysis, we have used the raw image mode data that were provided in ESO archive.[1] The preliminary data reduction was performed using the *Image Reduction and Analysis Facility* (IRAF[2]; Tody 1986, 1993) software. We have carried out the dark subtraction, flat-fielding, sky subtraction using each of the jittered images, and cosmic ray removal using the standard packages available in IRAF.

A close-up view of the representative *J*-band images for each of the objects LP 1033-31 and LP 877-72 is shown in Fig. 1, where the usual conventions were followed, i.e. north is up, and east is left. Both LP 1033-31 and LP 877-72 are clearly resolved as a binary with two components. In the case of LP 1033-31, the components have almost equal brightness with a slightly higher flux of the south-east component (LP 1033-31 A) than the north-west component (LP 1033-31 B). However, LP 877-72 consists of two components having very different brightness, where the north-west component (LP 877-72 A) is clearly observable as the brighter one than the south-east component (LP 877-72 B). In our analysis, we have taken the brighter component as primary.

We have measured the CCD chip coordinates (i.e. positions) of the sources on each of the science images using the PYTHON task DAOSTARFINDER (Stetson 1987) available in PHOTUTILS package. The task DAOSTARFINDER finds the object centroid by fitting the marginal x and y one-dimensional distributions of Gaussian kernel to the marginal x and y distributions of the unconvolved image. The separation between the centroids of the primary and secondary components was derived for each of the science images. The derived separations for both the objects in all JHK_s images are given in the 2nd, 6th, and 10th columns of Table 1. The binary separations are found to be consistent for both the sources. For LP 1033-31, we derive a separation of 402 ± 1, 401 ± 1, and 401 ± 1 mas for JHK_s photometric bands, whereas for LP 877-72, these values are calculated to be 1354 ± 2, 1355 ± 2, and 1356 ± 2 mas, respectively. Using the PYTHON package ASTROPY, we have converted all the pixel coordinates to World Coordinate System, whereas in order to derive the PAs of each of the images, we have used the PYASTRONOMY package. The derived values of PA of the secondary with respect to the primary components are listed in 3rd, 7th, and 11th columns of Table 1 for *J*, *H*, and K_s bands, respectively. These values show consistency for both the sources. The calculated values of PA for LP 1033-31 are 333.99° ± 0.16°, 333.95° ± 0.10°, and 334.07° ± 0.10° for JHK_s photometric bands, whereas in case of LP 877-72, the PAs were derived to be 138.52° ± 0.06°, 138.60° ± 0.05°, and 138.68 ± 0.10°, respectively.

[1] https://archive.eso.org/eso/eso_archive_main.html
[2] http://iraf.net

Table 1. Binary separation, position angle, and flux-ratio measurements for the observed 60 images for LP 1033-31 and 90 images for LP 877-72.

#	*J* band Separation (mas)	*J* band PA	*J* band Flux ratio	#	*H* band Separation (mas)	*H* band PA	*H* band Flux ratio	#	K_s band Separation (mas)	K_s band PA	K_s band Flux ratio
					LP 1033-31						
1	398.4	334.08°	1.06 ± 0.03	1	402.7	333.94°	1.07 ± 0.04	1	400.5	334.04°	1.08 ± 0.04
2	400.8	333.83°	1.06 ± 0.07	2	399.9	333.76°	1.07 ± 0.02	2	402.0	334.14°	1.07 ± 0.03
3	402.3	334.14°	1.07 ± 0.03	3	399.6	333.94°	1.07 ± 0.09	3	400.0	333.99°	1.05 ± 0.09
4	401.6	333.91°	1.06 ± 0.07	4	401.7	334.21°	1.07 ± 0.05	4	400.3	334.09°	1.07 ± 0.08
5	402.4	334.46°	1.06 ± 0.03	5	402.7	333.90°	1.07 ± 0.03	5	399.0	334.17°	1.05 ± 0.07
6	401.1	334.13°	1.06 ± 0.08	6	400.8	334.09°	1.06 ± 0.03	6	402.4	334.07°	1.06 ± 0.06
7	402.2	334.12°	1.07 ± 0.04	7	399.7	333.99°	1.07 ± 0.04	7	400.8	334.06°	1.06 ± 0.06
8	403.6	333.96°	1.05 ± 0.04	8	400.8	333.96°	1.07 ± 0.04	8	400.2	333.96°	1.07 ± 0.05
9	403.4	333.97°	1.08 ± 0.03	9	399.8	333.91°	1.06 ± 0.08	9	402.5	334.08°	1.06 ± 0.08
10	403.3	334.02°	1.07 ± 0.03	10	400.0	334.04°	1.06 ± 0.04	10	402.4	333.92°	1.07 ± 0.07
11	404.8	334.13°	1.07 ± 0.04	11	400.2	334.04°	1.08 ± 0.05	11	402.0	334.04°	1.06 ± 0.04
12	400.8	333.92°	1.06 ± 0.06	12	403.4	333.80°	1.06 ± 0.03	12	401.1	334.09°	1.06 ± 0.08
13	403.8	333.91°	1.07 ± 0.04	13	400.6	333.84°	1.06 ± 0.09	13	400.9	334.30°	1.05 ± 0.13
14	400.5	333.98°	1.07 ± 0.04	14	401.9	334.03°	1.06 ± 0.04	14	402.1	333.88°	1.05 ± 0.04
15	403.1	333.93°	1.06 ± 0.04	15	400.1	334.01°	1.07 ± 0.04	15	402.0	334.13°	1.06 ± 0.06
16	403.8	333.79°	1.06 ± 0.03	16	402.1	333.92°	1.06 ± 0.03	16	402.7	334.11°	1.07 ± 0.04
17	402.9	333.66°	1.07 ± 0.03	17	401.5	333.86°	1.06 ± 0.04	17	401.8	333.94°	1.07 ± 0.03
18	401.2	334.07°	1.08 ± 0.08	18	402.9	333.91°	1.07 ± 0.03	18	400.3	334.21°	1.06 ± 0.11
19	402.6	333.91°	1.05 ± 0.04	19	400.7	333.97°	1.07 ± 0.04	19	400.1	334.18°	1.05 ± 0.08
20	400.6	333.86°	1.06 ± 0.03	20	401.7	333.89°	1.06 ± 0.06	20	401.4	334.06°	1.06 ± 0.06
					LP 877-72						
1	1353.4	138.52°	4.82 ± 0.36	1	1356.2	138.64°	4.74 ± 0.27	1	1355.0	138.71°	4.26 ± 0.26
2	1354.5	138.58°	4.57 ± 0.28	2	1356.6	138.62°	4.63 ± 0.34	2	1357.6	138.85°	3.86 ± 0.25
3	1354.8	138.58°	4.77 ± 0.30	3	1355.9	138.59°	4.64 ± 0.35	3	1357.0	138.85°	4.12 ± 0.26
4	1354.6	138.45°	4.57 ± 0.36	4	1354.9	138.67°	4.66 ± 0.33	4	1356.4	138.68°	4.16 ± 0.26
5	1356.2	138.48°	4.66 ± 0.30	5	1357.4	138.52°	4.81 ± 0.35	5	1356.7	138.76°	4.11 ± 0.25
6	1354.8	138.54°	4.62 ± 0.33	6	1356.1	138.55°	4.66 ± 0.34	6	1356.7	138.63°	4.18 ± 0.26
7	1351.0	138.57°	4.62 ± 0.31	7	1353.0	138.55°	4.66 ± 0.34	7	1358.2	138.84°	4.13 ± 0.26
8	1353.3	138.49°	4.64 ± 0.35	8	1355.4	138.61°	4.52 ± 0.42	8	1357.9	138.75°	4.08 ± 0.26
9	1354.3	138.53°	4.86 ± 0.36	9	1353.3	138.63°	4.74 ± 0.35	9	1359.2	138.86°	3.99 ± 0.27
10	1351.9	138.62°	4.66 ± 0.37	10	1356.2	138.56°	4.49 ± 0.37	10	1354.0	138.59°	4.26 ± 0.26
11	1353.6	138.52°	4.76 ± 0.36	11	1356.1	138.62°	4.51 ± 0.35	11	1357.1	138.82°	4.13 ± 0.25
12	1354.4	138.57°	4.61 ± 0.22	12	1353.9	138.56°	4.87 ± 0.27	12	1357.4	138.81°	4.07 ± 0.25
13	1353.1	138.51°	4.88 ± 0.37	13	1357.0	138.59°	4.70 ± 0.37	13	1356.2	138.75°	4.02 ± 0.24
14	1353.4	138.69°	4.76 ± 0.40	14	1356.8	138.59°	4.68 ± 0.38	14	1355.0	138.76°	4.06 ± 0.26
15	1349.1	138.39°	4.62 ± 0.37	15	1353.4	138.70°	4.89 ± 0.28	15	1356.2	138.59°	4.12 ± 0.26
16	1352.8	138.44°	4.92 ± 0.37	16	1356.2	138.58°	4.48 ± 0.33	16	1354.6	138.70°	4.11 ± 0.26
17	1355.0	138.50°	4.87 ± 0.31	17	1353.1	138.58°	4.68 ± 0.33	17	1354.9	138.73°	4.16 ± 0.26
18	1356.3	138.53°	4.96 ± 0.38	18	1351.6	138.52°	4.58 ± 0.33	18	1354.1	138.59°	4.15 ± 0.27
19	1355.0	138.49°	4.56 ± 0.23	19	1354.9	138.62°	4.36 ± 0.31	19	1355.2	138.63°	4.13 ± 0.27
20	1354.9	138.53°	4.86 ± 0.30	20	1352.5	138.56°	4.58 ± 0.34	20	1350.7	138.51°	4.07 ± 0.28
21	1352.4	138.47°	4.72 ± 0.31	21	1355.1	138.67°	4.58 ± 0.41	21	1354.4	138.53°	4.13 ± 0.28
22	1354.5	138.57°	5.02 ± 0.29	22	1357.8	138.58°	4.44 ± 0.33	22	1358.4	138.68°	4.12 ± 0.27
23	1351.4	138.49°	4.82 ± 0.35	23	1354.6	138.48°	4.30 ± 0.33	23	1351.7	138.60°	4.15 ± 0.28
24	1354.7	138.57°	5.10 ± 0.29	24	1356.2	138.58°	4.38 ± 0.31	24	1354.6	138.56°	4.16 ± 0.25
25	1353.9	138.44°	4.95 ± 0.23	25	1355.2	138.60°	4.38 ± 0.33	25	1352.5	138.64°	4.10 ± 0.26
26	1349.6	138.41°	4.56 ± 0.24	26	1353.2	138.66°	4.35 ± 0.40	26	1355.7	138.63°	4.12 ± 0.27
27	1352.4	138.45°	4.74 ± 0.29	27	1356.7	138.55°	4.31 ± 0.31	27	1355.4	138.57°	4.01 ± 0.25
28	1355.2	138.48°	4.95 ± 0.38	28	1358.1	138.59°	4.39 ± 0.38	28	1353.0	138.63°	4.14 ± 0.27
29	1352.5	138.57°	4.64 ± 0.30	29	1353.3	138.59°	4.47 ± 0.35	29	1355.2	138.65°	4.14 ± 0.26
30	1352.6	138.47°	4.70 ± 0.43	30	1352.6	138.61°	4.41 ± 0.34	30	1354.4	138.63°	4.12 ± 0.21

In order to derive the flux ratio and the instrumental magnitude, aperture photometry was performed on both the components in each frame for both the sources LP 1033-31 and LP 877-72. Using the IRAF task PHOT, we properly centre the source, and with the given radius of the aperture as input, it derives the background-subtracted sum of all the photons within that aperture. This task also allows us to specify a series of the increasing aperture from an optimal small aperture (FWHM of the source profile) to a larger aperture (10 times of the FWHM). The increment of the aperture was 0.5 pixel. The larger the aperture, the more the flux of the source would be enclosed by the aperture. However, with a larger aperture, the errors introduced due to sky subtraction would also be larger.

Theoretically, a stellar (Gaussian) profile extends up to infinity. Therefore, the magnitude that is restricted for the chosen aperture

Table 2. Measured parameters of the two VLM systems LP 1033-31 and LP 877-72.

Binaries	LP 1033-31			LP 877-72		
	2MASS	Individual components		2MASS	Individual components	
Parameter	A+B	A	B	A+B	A	B
J	9.10 ± 0.02	9.82 ± 0.04	9.90 ± 0.04	8.86 ± 0.02	9.08 ± 0.03	10.77 ± 0.04
H	8.47 ± 0.02	9.24 ± 0.03	9.40 ± 0.03	8.24 ± 0.04	8.46 ± 0.04	10.11 ± 0.05
K_s	8.21 ± 0.02	9.01 ± 0.05	9.08 ± 0.05	8.00 ± 0.02	8.24 ± 0.02	9.77 ± 0.03
G^a		–	–		11.818	13.381
M_J		8.7 ± 0.4	8.8 ± 0.4		6.44 ± 0.03	8.13 ± 0.04
M_H		8.1 ± 0.4	8.2 ± 0.4		5.82 ± 0.04	7.47 ± 0.05
M_{Ks}		7.8 ± 0.4	7.9 ± 0.4		5.60 ± 0.02	7.13 ± 0.03
M_G		–	–		10.721	12.284
$J - K_s$	0.81 ± 0.06	0.82 ± 0.06	0.89 ± 0.03	0.87 ± 0.03	0.84 ± 0.03	1.00 ± 0.05
ΔJ		0.08 ± 0.06			1.69 ± 0.03	
ΔH		0.16 ± 0.04			1.65 ± 0.04	
ΔK_s		0.07 ± 0.06			1.54 ± 0.02	
SpT^b	M4	M4.5 ± 0.5	M4.5 ± 0.5	M4	M1.0 ± 0.3	M3.8 ± 0.3
Position angle		$334.0^\circ \pm 0.1^\circ$			$138.6^\circ \pm 0.1^\circ$	
Separation (mas)		402 ± 1			1355 ± 2	

[a] *Gaia* DR2 magnitude. [b]Spectral type of combined system is adopted from Rajpurohit et al. (2013). For the individual systems, the spectral types have been derived from M_J using the method of Scholz et al. (2005).

needs to be corrected for the excess counts in the wings of the stellar profile. The correction from profile fitting magnitude to aperture magnitude is carried out by the process of determining the aperture growth curve, i.e. a plot of magnitude within a given aperture versus aperture size. The aperture correction is simply the magnitude difference between the asymptotic magnitude and the magnitude at the given aperture. The most straightforward way to determine the aperture correction is to measure it directly from a number of growth curves. A more advanced method for doing the aperture correction is the DAOGROW algorithm (Stetson 1990), implemented in the IRAF task MKAPFILE in the package DIGIPHOT.PHOTCAL. Using this task, a stellar profile model was fitted to the growth curves for one or more components in one or more images. It then computes the aperture correction from a given aperture to the largest aperture. Again, we also took great care that the neighbouring components would not start influencing the sky background of the selected component. In order to do that, we have plotted the intensity variation along the axis (line joining the centroid of both components). We have taken the minimum intensity of this plot as the upper limit of aperture. In each frame, we again verified manually to avoid any unwanted mistake, and the optimal aperture is selected.

4 RESULTS

4.1 NIR photometry

Using the procedure described in Section 3, we have estimated the instrumental magnitudes, which were then standardized to apparent magnitude using the zero-point images that were routinely taken for NaCo service operation. The results for individual J, H, and K_s bands apparent magnitudes are summarized in the first three rows of Table 2. We have also estimated the flux ratio as the ratio of the flux of primary to secondary components in each of the frames. The results are shown in 4th, 8th, and 12th columns of Table 1 for J, H, and K_s bands, respectively. The uncertainties in flux ratios that are shown in the table were estimated using the propagation of the photometric uncertainty.

The photometric measurements for the unresolved combined system of LP 1033-31 and LP 877-72 in J, H, and K_s bands were available from the 2MASS data. The 2MASS magnitudes of LP 1033-31 and LP 877-72 reflect the combined flux from both components. In order to carry out a more robust analysis, we have also derived the magnitude of the individual components from the combined flux and the flux ratio as derived in Table 1. We found that the apparent magnitudes derived in this method are consistent with our photometric analysis within 2σ. In the case of LP 877-72, the detection of the components of LP 877-72 A and B confirms the observations from *Gaia* DR2 (Bailer-Jones et al. 2018). The binary separation and PA derived in this work also match with the results from *Gaia*; however, previous authors did not calculate detailed astrometry. The individual *Gaia* magnitudes of LP 877-72 AB were $G = 11.82$ and 13.38, respectively, for the A and B components.

As discussed in Section 1, following Finch et al. (2014) and Bailer-Jones et al. (2018), in this work we have adopted the distances for LP 1033-31 and LP 877-72 as 16.57 ± 3.27 and 33.77 ± 0.17 pc, respectively. In order to assign the above-measured distances as the distance of individual spatially separated components (A and B) of LP 1033-31 AB and LP 877-72 AB, it is important to be sure that the A and B components really comprise a true binary system, rather than an unrelated pair with a small projected separation. In our analysis, the $J-K_s$ colour and derived spectral type for both the components in each of the systems LP 1033-31 AB and LP 877-72 AB are found to have similar values within $1–2\sigma$ (see 9th row in Table 2). Since both the systems share the equal flux ratio and colour between the two individual components, the chance of either of the A or B component of the system for being a background object is very little and can be ruled out (Dahn et al. 2002; Hawley et al. 2002; West et al. 2008; Bonfini et al. 2009).

With the assumption that the two components (A and B) in each of the observed systems LP 1033-31 AB and LP 877-72 AB are indeed part of the physical binary systems (i.e. both components in each system are located at the same distance), the absolute magnitudes of the individual components can be determined for each individual components of the binary systems. The derived absolute magnitudes

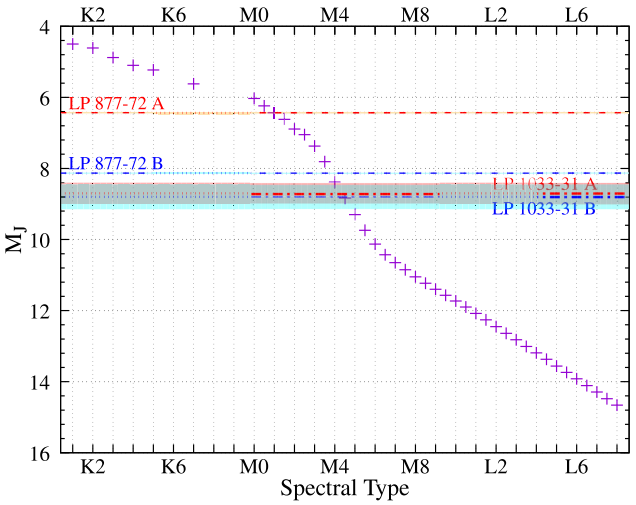

Figure 2. Absolute magnitude M_J as a function of spectral types adopted from Scholz et al. (2005) is shown by '+' symbol. The dashed and dot–dashed lines show the derived M_J of LP 877-72 AB and LP 1033-31 AB, respectively. The red and blue colours denote, respectively, the primary (A) and secondary (B) components of each system. The orange and cyan shades show the respective uncertainties in A and B components.

(M_J, M_H, M_{Ks}, and M_G) for both the systems in J, H, K_s, and G (only for LP 877-72) photometric bands are given in 5th–8th rows of Table 2. Due to the larger uncertainty in distance measurement for LP 1033-31 AB, the estimated uncertainties in the absolute magnitude of LP 1033-31 AB are derived to be approximately 10 times larger than the uncertainties in LP 877-72 AB.

4.2 Spectral classification

In recent years, several empirical relationships have been derived between the absolute J magnitude (M_J) and spectral type of the stars (e.g. Dahn et al. 2002; Cruz et al. 2003; Scholz et al. 2005). These relationships are very useful in order to estimate the spectral types of the individual stellar components of the VLM stars. In our analysis, we have used the new calibration from the empirical data of Scholz et al. (2005) to determine the spectral type. This is because unlike other methods, this relationship is applicable within a wide spectral range of K0–L8. Fig. 2 shows the relation of the spectral type and absolute magnitude M_J adopted from Scholz et al. (2005) along with the derived M_J of the individual components of LP 1033-31 AB and LP 877-72 AB with dashed and dot–dashed lines. We found that the spectral type of both LP 1033-31 A and B are similar within their uncertainty range and derived to be M4.5 ± 0.5. In the case of LP 877-72 A and B components, the derived spectral types are M1.0 ± 0.3 and M3.8 ± 0.3, respectively. The uncertainty in each case of spectral type was derived propagating the uncertainty of all involved parameters.

5 PHYSICAL PARAMETERS OF VLM BINARIES

5.1 Ages

Estimating the exact age for any of these binaries, LP 1033-31 and LP 877-72 are difficult since there are no Li measurements yet published (which could place an upper limit on the ages; see Zboril, Byrne & Rolleston 1997). Using the *Hipparcos* data, Caloi et al. (1999) have estimated the age of stellar populations in the solar neighbourhood (0.6–7.5 Gyr) and categorized the sample with respect to their velocity. Using the PM and distances as mentioned in Section 1, for LP 1033-31 and LP 877-72, we have estimated the tangential velocity of 23.48 and 48.82 km s^{-1}, respectively. This sets a lower limit to the age range of LP 1033-31 and LP 877-72 binary systems to be ≥0.01 and ≥1.5–2 Gyr, respectively (Caloi et al. 1999).

Since both the binary systems consist of M-dwarfs, we can get a crude estimation of the age of the individual components using the age-activity relation for M-dwarfs (West et al. 2008). Initially, considering the combined systems, both objects LP 1033-31 and LP 877-72 have combined spectral-type M4 (using 2MASS data; Rajpurohit et al. 2013), which corresponds to an age range of $4.5^{+0.5}_{-1.0}$ Gyr from the age-activity relation (West et al. 2008). However, considering the individual systems, the estimated age for both the primary and secondary components of LP 1033-31 would lie within the range of 3.5–7.5 Gyr or ≈5 Gyr. In case of LP 877-72, the individual components give quite different ages for primary and secondary (≲0.8 and 1.5–5.0 Gyr), which is unlikely for a physically bound system since both components of the binary system supposed to be created at the same age. Using the evolutionary calculations by Chabrier & Baraffe (1997) and Chabrier et al. (2000), the typical age for the mass range of ≳0.15 $M_\odot$ was estimated to be <10 Gyr (Chabrier & Baraffe 1997; Chabrier et al. 2000). It should be noted that there is little significant difference between the evolutionary tracks for ages 0.6–10 Gyr for these spectral types. Therefore, we have conservatively assumed that age of ∼5 Gyr.

5.2 Masses, surface gravities, and effective temperatures

Initially, we have estimated the masses of both the components of LP 1033-31 and LP 877-72 using the mass-absolute magnitude relation as derived by Benedict et al. (2016). From the K-band absolute magnitudes as derived in Section 4.1, we have estimated the mass of LP 1033-31 A and B to be 0.19 ± 0.04 and 0.18 ± 0.04 $M_\odot$, respectively. In case of LP 877-72, the respective values of masses of the primary and secondary are derived to be 0.565 ± 0.004 and 0.286 ± 0.005 $M_\odot$. In order to carry out a more robust analysis, we have also interpolated the Baraffe et al. (2015) isochrones for an age of 5 Gyr. LP 1033-31 AB are found to have the nearly equal mass of 0.20 ± 0.04 and 0.19 ± 0.04 $M_\odot$, whereas, for LP 877-72 AB, the derived masses are found to be 0.520 ± 0.006 and 0.260 ± 0.005 $M_\odot$, respectively. Although both the methods of estimating masses give similar results within 3σ and 5σ for LP 1033-31 and LP 877-72, we have used the later method of mass estimation for further analysis in this paper due to its robustness. The derived mass, $T_{\rm eff}$, and log g are given in Table 3. For LP 1033-31, the $T_{\rm eff}$ and log g are found to be similar, whereas in the case of LP 877-72, the primary is ∼400 K hotter and log g is ∼1.6 times less than the secondary component.

5.3 Stellar radii and luminosities

In order to derive the stellar radius for both the stars, we have used single-star mass-radius relations (Boyajian et al. 2012). The radii of LP 1033-31 A and B are derived to be 0.225 ± 0.030 and 0.217 ± 0.029 $R_\odot$. Whereas for LP 877-72 AB, the radius is estimated to be 0.492 ± 0.011 and 0.270 ± 0.006 $R_\odot$ for primary and secondary, respectively. Using the Stefan–Boltzmann law, we have estimated the luminosity of both the primary and secondary components of LP 1033-31 and LP 877-72 (see Table 3). Further, we have also derived the luminosity using the stellar luminosity versus temperature relation given by Boyajian et al. (2012). Both the methods are found to be consistent within its uncertainty level.

Table 3. System parameters for LP 1033-31 and LP 877-72 assuming the age of 5 Gyr.

Par[a]	LP 1033-31		LP 877-72	
	A	B	A	B
d	16.57 ± 3.27		33.77 ± 0.17	
a	6.7 ± 1.3		45.8 ± 0.3	
M	0.20 ± 0.04	0.19 ± 0.04	0.520 ± 0.006	0.260 ± 0.005
R	0.225 ± 0.030	0.217 ± 0.029	0.492 ± 0.011	0.270 ± 0.006
$T_{\rm eff}$	3245 ± 107	3211 ± 120	3750 ± 15	3348 ± 10
log g	5.061 ± 0.038	5.068 ± 0.039	4.768 ± 0.005	4.984 ± 0.004
L	0.0050 ± 0.0015	0.0045 ± 0.0014	0.0432 ± 0.0021	0.0082 ± 0.0004
P	28.0 ± 2.6		349.4 ± 2.5	
$E_{\rm Bind}$	−10.0 ± 3.5		−5.21 ± 0.12	

[a] The parameters in first column: d – distance in pc; a – binary separation in AU; M – mass in $M_\odot$ as derived from the interpolation of Baraffe et al. (2015) isochrones; R – radius in $R_\odot$; $T_{\rm eff}$ – effective temperature in K; log g – logarithmic value of surface gravity in cgs unit; L – luminosity in $L_\odot$; P – orbital period in yr; $E_{\rm Bind}$ – binding energy in 10^{43} erg.

5.4 Binary separations, orbital periods, and binding energies

In Section 3, we have derived the projected angular separation between the individual components (between A and B) of LP 1033-31 and LP 877-72 to be 402 ± 1 and 1355 ± 2 mas. Incorporating the distances taken from Bailer-Jones et al. (2018) and Finch et al. (2014), as discussed in Section 1, we derived the projected physical separation between the two systems of 6.7 ± 1.3 and 45.8 ± 0.3 AU, respectively. Because of the projection effects, the real separation between the components is expected to be, on average, 1.4 times larger (Couteau 1960). However, in this study, we have taken the measured projected separations and the masses derived in Section 5.2 to estimate the orbital periods for each of the systems. The orbital period derived for LP 1033-31 is found to be 28 ± 3 yr whereas for LP 877-72, it is derived to be 349 ± 3 yr. Therefore, none of our candidates will have measurable orbital motions and hence will have a common PM on the sky.

Since low-mass binary systems are expected to have low (absolute values of) gravitational potential (binding) energies, in order to understand if these systems are physically bound or not, we have calculated the binding energies for LP 1033-31 and LP 877-72. Using the masses and projected physical separations (instead of the true separations), the binding energies ($U = -G.M_1.M_2/r$, where M_1 and M_2 are the masses of the components and r is the distance between them) for LP 1033-31 and LP 877-72 are derived to be $-1.00 \pm 0.35 \times 10^{44}$ and $-5.21 \pm 0.12 \times 10^{43}$ erg, respectively. We have further discussed the stability of the systems in Section 6.5.

6 DISCUSSION

Using high-resolution NaCo/VLT images, we have detected and characterized two VLM binaries LP 1033-31 and LP 877-72. In this section, we have discussed how the understanding of these two sources has been changed through our study. We also discussed whether the identified components, in this study, match with other similar kinds of systems or not.

6.1 The detected binaries: previous and present understanding

In Section 4.2, we characterized both LP 1033-31 and LP 877-72 to be the VLM binaries and estimated the masses of each component of LP 1033-31 to be ∼0.2 $M_\odot$, whereas for primary and secondary of LP 877-72, the derived values of masses are 0.52 and 0.26 $M_\odot$. Using TIC catalogue, the latest values of masses for LP 1033-31 and LP 877-72 as 'single' objects were estimated to be 0.316 and 0.600 $M_\odot$ (Cloutier 2019; Stassun et al. 2019). Both of these values were found to be greater than masses of the individual components, however, slightly lower (within few σ uncertainty level) than the total estimated masses (M_A+M_B) in our study.

The radii of both LP 1033-31 and LP 877-72 were estimated by Stassun et al. (2019) to be 0.319 and 0.556 $R_\odot$, respectively. These values were larger than both of the primary and secondary components of each VLM binaries. Considering 'single' object, the latest values of log g and $T_{\rm eff}$ were estimated to be 4.93 and 3368 K for LP 1033-31 (Muirhead et al. 2018; Stassun et al. 2018), and 4.63 and 3782 K for LP 877-72 (Gaia Collaboration 2018; Anders et al. 2019). In our analysis, we found that log g and $T_{\rm eff}$ for both the newly discovered components of LP 1033-31 are within ∼1.5–3 σ of that derived in earlier studies. For LP 877-72, we found that the previously derived values of surface gravity and temperatures are more close to the brighter component (i.e. the primary). This could be due to the fact that the secondary component is 5.2 times less luminous and 1.53–1.69 mag less bright than the primary, and hence the contribution of the secondary component to the total flux is only ∼20 per cent.

6.2 Combined spectral fitting

Since the spectral type for each of the binary components of both the sources (LP 1033-31 and LP 877-72) is found to be different than those that were estimated in previous studies, we have performed a more robust analysis. Although we do not have the spectra for each of the individual components, the spectra of the unresolved systems for both LP 1033-31 and LP 877-72 were already been observed and studied by Reylé et al. (2006). We have used the latest available empirical template library of stellar spectra from Kesseli et al. (2017) and fitted the combined spectra at the flux ratios derived in the Section 3. Since the empirical template library of stellar spectra does not provide any fractional spectral class, we have combined the spectral types to estimate it from the nearest spectral classes (e.g. the spectra of spectral class M4.5 is derived averaging the spectral classes M4 and M5).

In Fig. 3, the combined spectra of LP 1033-31 (left) and LP 877-72 (right) are shown by blue solid lines that were observed by Reylé et al. (2006). Whereas the red solid line in each plot shows the combined template spectra of the primary and secondary using the derived spectral types in this study. In order to compare whether the derived spectral class, from our analysis, gives any better fit or not, we have also overplotted the best-fitting template spectra of the unresolved systems (green solid line). We have used the spectral class from Rajpurohit et al. (2013) as shown in Table 2. It is clearly evident that the fitting is better when the spectra of the individual components are combined. This might be due to the better understanding of the system after both the components get spatially resolved.

6.3 Mass ratios

Investigation of the binary mass ratios is very important since the mass-ratio distributions provide stringent tests for models of binary star formation (see El-Badry et al. 2019, and references therein). Most studies of binary stars fit a single power-law distribution $f_q \propto q^\gamma$ to the observed mass ratios (Shatsky & Tokovinin 2002; Sana et al. 2012; Duchêne & Kraus 2013; De Rosa et al. 2014). However, with large samples, it was noticed that a single-parameter model could not adequately fit the distribution across all mass ratios (Duquennoy & Mayor 1991; Halbwachs et al. 2003; Gullikson, Kraus & Dodson-Robinson 2016; Moe & Di Stefano 2017; Murphy et al. 2018; El-Badry et al. 2019), and hence a multiparameter power-law model was

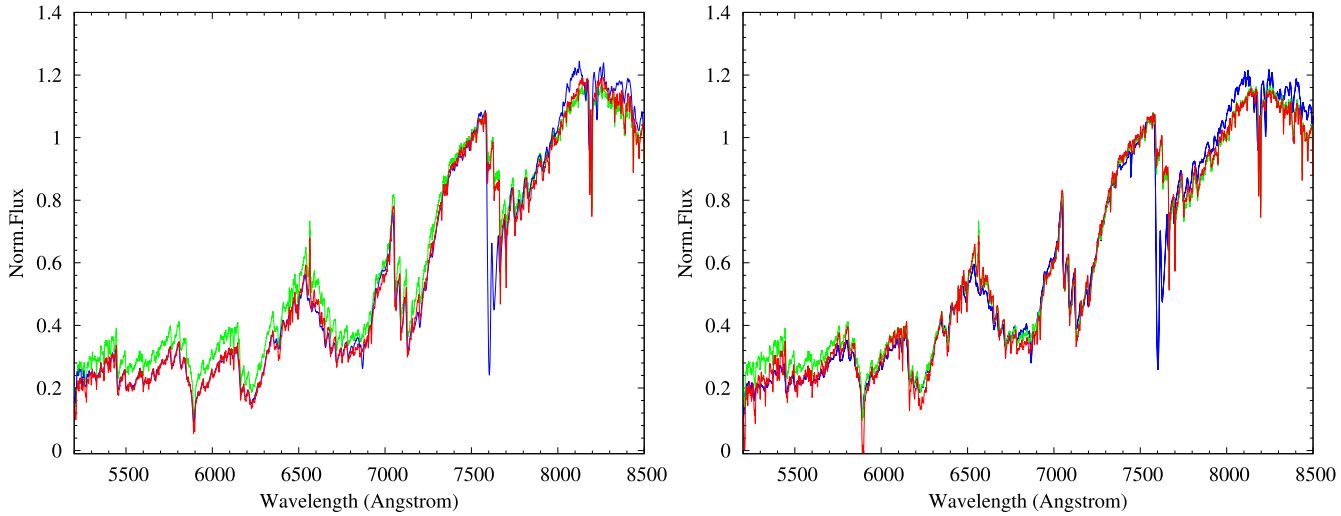

Figure 3. Combined template fit to the observed spectra. The observed 2MASS spectra of the unresolved systems LP 1033-31 (a) and LP 877-72 (b), adopted from Reylé et al. (2006), are shown with blue solid line. The best-fitting spectra created with the combination of the templates of the primary and secondary of each systems using the derived spectral types from our analysis (see Section 4.2) and in relevant flux ratios (as given in Table 1) have been shown with red solid line. We have adopted the latest template spectra as given by Kesseli et al. (2017). For comparison, we have also shown the best-fitting template spectra for the previously unresolved systems (green solid line) using the spectral types derived by Rajpurohit et al. (2013) (as mentioned in Table 2). This is clearly evident that the combined template fitting using the spectral type of the individual components from this study shows a better fit to the observed spectra than the spectra of the unresolved system.

adopted with different slopes (such as $\gamma_{\rm small-q}$ and $\gamma_{\rm large-q}$) across the small-to-large mass ratios. The values of the slopes also depend on the projected separations of the binaries as well as the spectral types of the individual components. Therefore, in order to provide observational constraints on the theoretical models, observations of mass ratios are necessary.

In this work, we have derived the mass ratios of LP 1033-31 and LP 877-72 to be 0.95 ± 0.28 and 0.50 ± 0.01, respectively. In a study of multiplicity among M-dwarfs, Fischer & Marcy (1992) found that the distribution of mass ratios is flat and perhaps declines at low-mass ratios. By analysing a catalogue of 1342 low-mass binaries with at least one mid-K to mid-M-dwarf component, Dhital et al. (2010) found the distribution of mass ratios to be strongly skewed toward equal-mass pairs: 85.5 per cent of pairs have masses within 50 per cent of each other. A similar result is obtained by Reid & Gizis (1997) in the volume-complete 8-pc sample, which includes mostly (80 per cent) of M-dwarfs. In recent years, M-dwarf binaries are weighted towards more equal masses (see Winters et al. 2019a, for a review). Fig. 4 shows the mass ratios of both the objects (LP 1033-31 and LP 877-72) with respect to the mass of the primary component. For a comparison with M-dwarfs, we have overplotted all the pairs in the sample taken by Winters et al. (2019a). For early M-dwarf binaries with intermediate separations a $\approx$10 AU, the mass-ratio distribution is nearly uniform with a turnover in the sub-stellar brown dwarf regime (Fischer & Marcy 1992; Bergfors et al. 2010; Janson et al. 2012; Winters et al. 2019a). For binaries with late M-dwarf primaries and intermediate separations $a \approx$1–10 AU, the mass-ratio distribution is weighted significantly towards $q \gtrsim 0.7$ (Bouy et al. 2003; Joergens 2006; Basri & Reiners 2006; Bergfors et al. 2010; Dieterich et al. 2012; Duchêne & Kraus 2013; Winters et al. 2019a). In this study, we also noticed a similar feature for LP 1033-31, which, having both components of spectral type M4.5, shows similar mass range. However, with an early-M-dwarf primary component, LP 877-72 shows a mass ratio of $\sim$0.5.

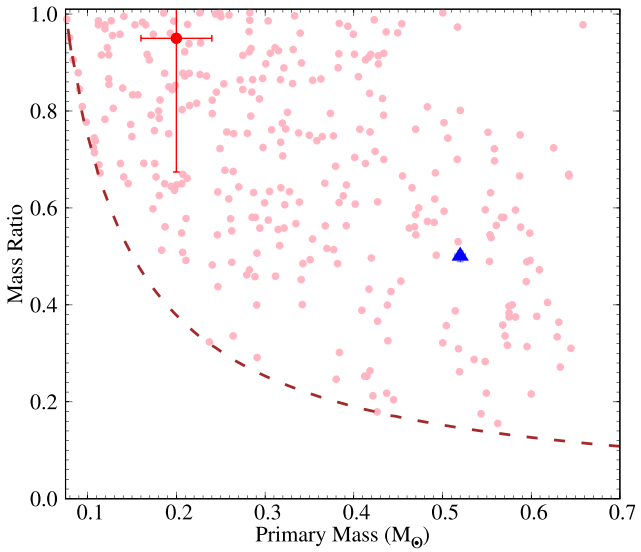

Figure 4. Mass ratio as a function of primary mass for LP 1033-31 AB and LP 877-72 AB has been shown with red solid circle and blue solid triangle, respectively. For comparison with other M-dwarf binaries, we have overplotted the data from the latest work of Winters et al. (2019a) with light-pink solid circle. The brown dashed line indicates the mass-ratio boundary relative to the lowest mass considered in their survey (i.e the hydrogen burning limit $M \gtrsim 0.075$ M$_\odot$).

6.4 Binary separation

In this work, we have estimated the binary separation of the binaries LP 1033-31 AB and LP 877-72 AB to be 6.7 ± 1.3 and 45.8 ± 0.03 AU, respectively (see Section 5.4). In a series of studies in solar neighbourhood M-dwarfs and VLM binaries, Fischer & Marcy (1992), Close et al. (2003), Gizis et al. (2003), and Siegler et al.

(2005) and few other authors have shown that the separation of the binary systems lies within a maximum separation of ∼30 AU. Close et al. (2003) have even investigated the reason behind the lack of wide ($a > 20$ AU, which was the observational upper limit of binary separation in their survey) VLM/brown dwarf binaries. They have suggested a possible significant differential velocity kick, as was predicted by the 'embryo ejection' theories. Their estimates also indicated that a fragmentation-produced VLM binary semimajor axis distribution contains a significant fraction of wide VLM binaries in contrast to their observation.

The first known VLM binary wider than 30 AU was discovered by Luhman (2004) with a projected separation $a \sim 240$ AU. In the later studies, more and more wide VLM binaries have been discovered and analysed by several authors, which includes the work of Chauvin et al. (2004) ($a \sim 55$ AU), Golimowski et al. (2004) ($a \sim 0.83$–30 AU), Phan-Bao et al. (2005) ($a \sim 33$ AU), Billères et al. (2005) ($a \sim 220$ AU), Law, Hodgkin & Mackay (2006) ($a \sim 10$–94 AU), Close et al. (2007) ($a \sim 212$–243 AU), Reid, Cruz & Allen (2007) ($a \sim 100$–3200 AU), Kraus & Hillenbrand (2007) ($a \sim 1600$ AU), Konopacky et al. (2007) (4 out of 13 binaries have $a > 100$ AU), Radigan et al. (2008) ($a \sim 135$ AU), Radigan et al. (2009) ($a \sim 6700$ AU), Kraus & Hillenbrand (2009) ($a \sim 500$–5000 AU), Bergfors et al. (2010) ($a \sim 3$–180 AU), Law et al. (2010) ($a \sim 600$–6500 AU), Janson et al. (2012) ($a \sim 3$–227 AU), Dieterich et al. (2012) ($a \sim 5$–70 AU), Janson et al. (2014) ($a \sim 0.4$–94 AU), Deacon et al. (2014) ($a \sim 300$–69 706 AU), Ward-Duong et al. (2015) ($a \sim 3$–10 000 AU), Cortés-Contreras et al. (2017) ($a \sim 1$–66 AU), Gálvez-Ortiz et al. (2017) ($a \sim 200$–92 000 AU), and Winters et al. (2019a) ($a \sim 10^{-2}$–10^4 AU). These discoveries of very wide separations of VLM binaries have been tried to explain recently with several models including the state of the art embrio-ejection scenario (Boss 2001; Reipurth & Clarke 2001). Numerical simulations have produced results that have led to claims related to binary formation via ejection (Bate, Bonnell & Bromm 2003; Umbreit et al. 2005).

Recently, Riaz, Vanaverbeke & Schleicher (2018) using the numerical simulations have attempted to model the initial stages of the formation of unequal mass brown dwarf and VLM systems evolving within a common envelope of gas. Starting from molecular cloud cores with various rotation rates and considering non-axisymmetric density perturbations to mimic the presence of large-scale turbulence on the level of molecular cloud cores, authors have successfully addressed the formation of wide VLM and brown dwarf binaries with semimajor axis up to 441 AU. It is to be noted that, since the binary separations for both of the binaries discussed in this paper (i.e. LP 1033-31 AB and LP 877-72 AB) range below this limit, the formation mechanism of both of them could be well explained with this scheme. However, as discussed above, many of the VLM binaries discovered in recent years have a binary separation wider than 441 AU. Therefore, those binaries could not be explained through the scheme of Riaz et al. (2018). That might be due to the fact that the simulations of Riaz et al. (2018) did not take into account for radiative feedback effects on the collapsing gas, which have a profound impact on the star-forming gas (Offner et al. 2009; Bate 2012; Myers et al. 2014; Krumholz et al. 2016). Further theoretical development is required in this context.

In Fig. 5, we have shown the separations of the VLM binaries LP 1033-31 and LP 877-72 with red and blue solid vertical lines, respectively. We have also overplotted the separation–distribution of few latest works on VLM binaries. With the increase in the number of VLM binaries over the years, the peak of the separation distribution has also been changed. The studies of Fischer & Marcy (1992), Close et al. (2003), Gizis et al. (2003), and Siegler et al. (2005) indicated

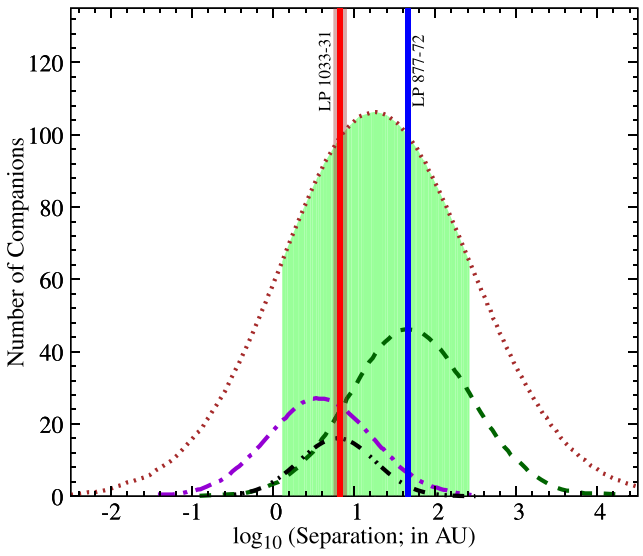

Figure 5. The projected separations of the binaries LP 1033-31 AB and LP 877-72 AB have been shown with the red and blue solid vertical lines, respectively. The semitransparent shades with same colours show the respective estimated uncertainties. The uncertainties for LP 1033-31 AB are clearly noticeable, whereas for LP 877-72 AB, the extent of uncertainties is smaller than the size of the line width. For comparison, the separation distributions of early- and mid-M-dwarf binaries estimated by Janson et al. (2014) have been shown by black dot-dot–dashed line and have a peak at ∼6 AU. For a larger sample of M-dwarf binaries, the distributions within 10 pc and 25 pc estimated by Winters et al. (2019a) have been shown with violet dot–dashed line (peak ∼4 AU) and brown dotted line (peak ∼20 AU), respectively. The semitransparent green-shaded region under the brown dotted line indicates the $\sigma_{\log a} = 1.16$, for the sample within 25 pc, as adopted from Winters et al. (2019a). The dark-green dashed line shows the fit for solar-type stars from Raghavan et al. (2010), which peaks at ∼51 AU.

that the peak of the distribution of separation of VLM binaries is ∼4 AU. For a sample of $0.1\,M_\odot \lesssim M \lesssim 0.5M_\odot$, Duchêne & Kraus (2013) have derived a peak of separation distribution to be ∼5.3 AU. Recent studies of Janson et al. (2014) (see Fig. 5; black dot-dot–dashed line) show a distribution peak of ∼6 AU, whereas Winters et al. (2019a) with the confirmed 290 samples within 25 pc (see Fig. 5; brown dotted line) have derived the peak of the separation distribution to be ∼20 AU. However, while taking a sub-sample of the stars lies within the 10-pc distance in solar neighbourhood (see Fig. 5; violet dot–dashed line), authors have noticed that the distribution peak shifts to the value at ∼4 AU. In this analysis, the VLM binaries we have reported are within $1\sigma_{\log a}$ of the total sample of the latest distribution of VLM binaries (see the green-shaded region in Fig. 5). For comparison, in Fig. 5, we have also plotted the separation distribution for solar-type stars (peak ∼51 AU; Raghavan et al. 2010). Although the peak of solar-type stars also comes within the $1\sigma_{\log a}$, the separation of LP 877-72 AB is nearer to this value.

6.5 Stability of the binary systems

Several studies have been carried out over the last few decades to investigate the stability of the binary systems in both theoretical and observational points of view. In Fig. 6, we plot the diagram of total mass versus the binding energy (a) and total mass versus binary separation (b). In both the plots, same symbols have been used. The binaries LP 1033-31 and LP 877-72 have been shown with a red solid circle and blue solid triangle. In the case of LP 877-72, the

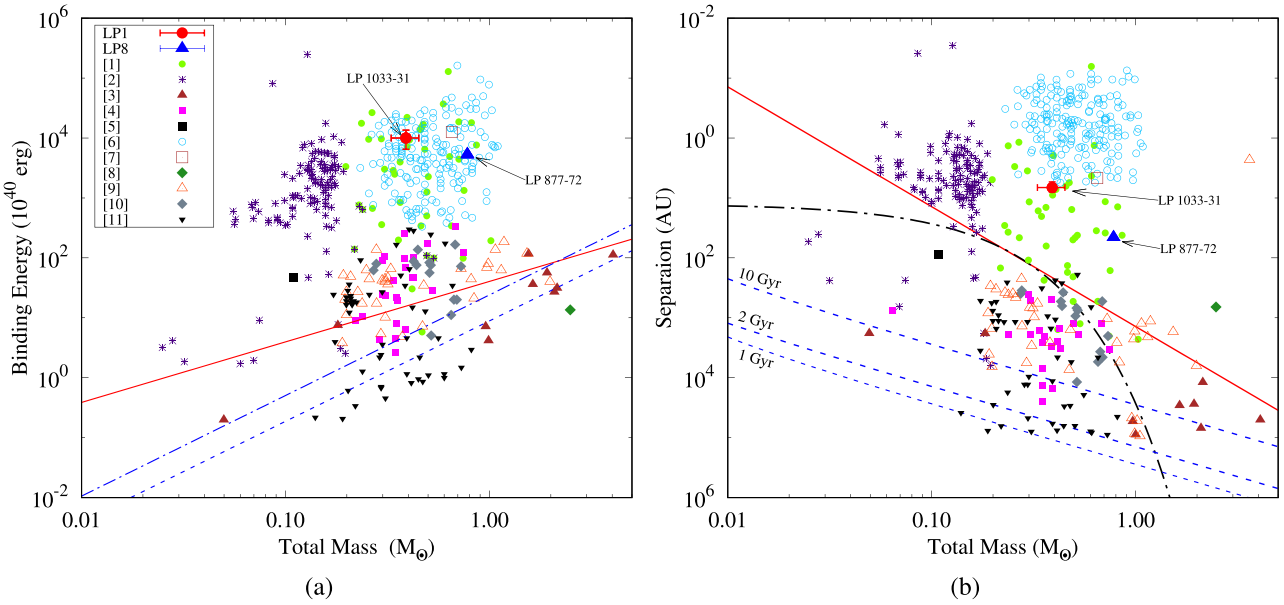

Figure 6. (a) System Binding Energy versus Total Mass (primary + secondary) and (b) Binary Separation versus Total Mass is shown. The detected binary systems LP 1033-31 AB (shown as LP1) and LP 877-72 AB (shown as LP8) have been shown with red solid circle and blue solid triangle, whereas the known binary systems from the literature are marked with different symbols. The estimated uncertainties have also shown for both the systems. For LP 1033-31 AB, the uncertainties are clearly visible, whereas for LP 877-72 AB, the uncertainties are smaller than the size of the symbols. Figure legend: [1]: Fischer & Marcy (1992) and Reid & Gizis (1997); [2]: VML archive, Burgasser et al. (2007b) and Siegler et al. (2005); [3]: Caballero et al. (2006) and Caballero (2007a, b, 2009); [4]: Luhman et al. (2009), Luhman (2012), Dhital et al. (2010), and Mužić et al. (2012); [5]: Burningham et al. (2010); [6]: Faherty et al. (2010) and Baron et al. (2015); [7]: Ross 458 AB, Beuzit et al. (2004) and Goldman et al. (2010); [8]: HIP 78530 AB, Lafrenière et al. (2011); [9]: Janson et al. (2012); [10]: Deacon et al. (2014); and [11]: Gálvez-Ortiz et al. (2017). In the panel (a), we have overplotted the minimum binding energy line from Zuckerman & Song (2009) (red solid line) and the two lines showing the Jeans length criteria for mass ratio $q = 1.0$ (blue dot–dashed line) and $q = 0.1$ (blue–dashed line) adopted from Faherty et al. (2010). In the panel (b), the empirical limit for stability stated by Reid et al. (2001) (black dot–dashed line) and by Burgasser et al. (2003) (red solid line) has been shown. We also overplot the lifetime isochrones suggested by Dhital et al. (2010) with data of Close et al. (2007) and Weinberg et al. (1987) equations for dissipation times of 1, 2, and 10 Gyr (blue dashed lines). Both the systems LP 1033-31 AB and LP 877-72 AB being well above the minimum-binding energy lines in (a) as well as the stability limits in (b) signify that both systems are stable.

sizes of the error bars are smaller than the sizes of the symbols. We have also overplotted other M-dwarf binaries as well as VLM binaries in order to compare them with LP 1033-31 and LP 877-72. By close inspection, it is clear from both the figures that the values of LP 1033-31 and LP 877-72 have more similarities to the studies by Fischer & Marcy (1992), Reid & Gizis (1997), Beuzit et al. (2004), Faherty et al. (2010), and Baron et al. (2015). That would be due to the fact that both of these sources have similar spectral types and also have the same properties of the solar neighbourhood.

Zuckerman & Song (2009) derived a cutoff for the binding energy of a system formed by fragmentation as a function of the total system mass. In this calculation, authors assumed the binary separations of 300 AU. However, due to the findings of number systems having separations larger than 300 AU, Faherty et al. (2010) used the Jeans length instead of the fiducial value of 300 AU to repeat the calculation for two extreme mass ratio cases. In Fig. 6(a), we have shown the binding energy cutoff estimated by Zuckerman & Song (2009) (red solid line) and Faherty et al. (2010) (blue dashed line for mass ratio = 0.1, and blue dot–dashed lines for mass ratio = 1.0). Both LP 1033-31 and LP 877-72 are found above the Zuckerman & Song (2009) and Faherty et al. (2010) limits of bound systems.

Further, in Fig. 6(b), we have also shown the suggested empirical limits for the stability of VLM multiples from the studies of Reid et al. (2001) (black dashed line), and Burgasser et al. (2003) (red solid line), based on the objects that were known at the time of the respective works. However, none of these cutoffs seems to be appropriate for the collection of widely separated systems (see Faherty et al. 2010). Later Dhital et al. (2010) applied Galactic disc mass density (Close et al. 2007) and other updated parameters to Weinberg, Shapiro & Wasserman (1987) equations and described statistically the widest binary that is surviving at a given age. In the Fig. 6(b), we have also overplotted the lifetime 'isochrones' suggested by Dhital et al. (2010) for the dissipation times of 1, 2, and 10 Gyr (blue dashed lines). With the parameters calculated in the previous sections, both systems LP 1033-31 and LP 877-72 appear to be stable enough to survive longer than 10 Gyr.

6.6 Possibility of hosting exoplanets

In this section, we have discussed the possibility of hosting exoplanet on the identified VLM components using the latest investigations on similar type of stars. Utilizing the M-dwarf surveys conducted with the HIRES/Keck, PFS/Magellan, HARPS/ESO, and UVES/VLT instruments supported with data from several other instruments, Tuomi et al. (2019) analysed the radial velocities of an approximate volume- and a brightness-limited sample of 426 nearby M-dwarfs and estimated that M-dwarfs (M0–M9.5) have, on average, at least $2.39^{+4.58}_{-1.36}$ planets per star orbiting them. Using *Kepler* data, Hardegree-Ullman et al. (2019) have also derived the planet occurrence rate specifically for mid-M-dwarfs (spectral types M3 V to M5.5 V) to be $1.19^{+0.70}_{-0.49}$. Hardegree-Ullman et al. (2019) also estimated the planet occurrence rate for smaller ranges of spectral types M3 V–M3.5 V, M4 V–M4.5 V, and M5 V–M5.5 V to be $0.86^{+1.32}_{-0.68}$, $1.36^{+2.30}_{-1.02}$, and $3.07^{+5.49}_{-2.49}$ planets per star. Since the estimated values of planet occurrence rate

by Hardegree-Ullman et al. (2019) show an increasing trend for larger spectral type, we might expect that for the spectral type >M5.5, the planet occurrence rate would be $\gtrsim$3.07 planets per star. Similarly, we also expect the planet occurrence rate for spectral types M_1 and M_2, to be lower than that was derived for spectral type M_3 (i.e. the rate for planet occurrence would be $\lesssim$0.86 planets per star).

In order to estimate the possibility of hosting planets for the detected VLM binaries, we first considered the planet occurrence rate for the individual components for each VLM binaries. After that we have also evaluated the effects of the binarity for each of the components. Considering the spectral types of LP 1033-31 A (∼M4.5), LP 1033-31 B (∼M4.5), LP 877-72 A (∼M1), and LP 877-72 B (∼M4), the planet occurrence rate would have been 0.34–3.66, 0.34–3.66, $\lesssim$0.86, and 0.34–3.66 planets per star. However, Wang et al. (2014) and Kraus et al. (2016) found that close binary companions appear to suppress planet formation and hence decrease planet occurrence rates for these systems. Recently, Moe & Kratter (2019) have compiled the recent works by Wang et al. (2014), Wang et al. (2015a), Wang et al. (2015b), Kraus et al. (2016), Ngo et al. (2016), Matson et al. (2018), and Ziegler et al. (2020), and have derived the relationship between the suppression factor (S_{bin}) as a function of binary separation. Using this relationship (see fig. 3 of Moe & Kratter 2019), we have estimated the values of the S_{bin} to be 0.126 ± 0.013 and 0.5708 ± 0.0018 for LP 1033-31 AB and LP 877-72 AB, respectively. Therefore, considering the suppression due to the binarity, for each of the primary and secondary components of LP 1033-31 AB, we derive that the probability of occurring planet would be the same and with the range of 4–51 per cent. In the case of LP 877-72, the primary and secondary components of the planet occurrence rate would be $\lesssim$49 per cent and 19–208 per cent. This means that, if we search for exoplanets around each of the components of the VLM binaries reported in this paper, we should expect to find up to 'two' exoplanets around LP 877-72 B; in contrast with the LP 877-72 A, LP 1033-31 A, and LP 1033-31 B, all three of the components that have the maximum probability of hosting exoplanet are only ∼50 per cent.

7 SUMMARY AND CONCLUSIONS

In this paper, we have presented a detailed study of two sources LP 1033-31 and LP 877-72, one of which was previously known as a single star (LP 1033-31), whereas another source (LP 877-72) was recently resolved into two components by *Gaia*. However, the properties of the newly discovered components were not well studied. Using the observations from NaCo/VLT high-resolution AO imaging in NIR JHK_s band, we found that LP 1033-31 consists of two components that have similar brightness, mass, radius, $T_{\rm eff}$, log g, and luminosity (within its $\sim 1\,\sigma$ uncertainties). However, in case of LP 877-72, these parameters are found to vary between the primary and secondary over a wide range. We have also investigated the properties of the binary systems, and the results are summarized below:

(i) The PA and the projected physical separation of LP 1033-31 AB are derived to be $334.01^\circ \pm 0.12^\circ$ and 6.7 ± 1.3 AU. The same parameters for LP 877-72 are estimated to be $138.60^\circ \pm 0.07^\circ$ and 45.8 ± 0.3 AU, respectively.

(ii) The spectral types for both the primary and secondary of LP 1033-31 AB are found to be similar and estimated to be M4.5. Whereas for LP 877-72 AB, the spectral types of the primary and secondary components are derived to be ∼M1 and ∼M4.

(iii) The system LP 1033-31 AB is found to have two nearly equal mass components with the estimated masses of 0.20 ± 0.04 and 0.19 ± 0.04 $M_\odot$. Whereas for LP 877-72 AB, the masses are estimated to be 0.520 ± 006 and 0.260 ± 0.006 $M_\odot$.

(iv) The primary and secondary components of LP 1033-31 AB are found to have similar radius and luminosity, with the values of ∼0.22 $R_\odot$ and ∼0.005 $L_\odot$, respectively. Whereas for LP 877-72, the radius of the primary is twice the radius of the secondary with the values of ∼0.49 and ∼0.27 $R_\odot$. However, the primary is five times more luminous than the secondary of LP 877-72 AB, with the luminosity of the primary to be ∼0.043 $L_\odot$.

(v) For LP 1033-31, the $T_{\rm eff}$ and log g are found to be similar with the values of ∼3200 K and ∼5.06. In the case of LP 877-72, the $T_{\rm eff}$ of the primary is ∼3750 K, which is ∼400 K hotter than the secondary component. The log g of the secondary component is found to be 1.05 times more than the primary component with a log g of the primary being 4.768.

(vi) The orbital periods of LP 1033-31 and LP 877-72 are also estimated to be 28 ± 3 and 349 ± 3 yr, respectively. We have estimated the binding energy for LP 1033-31 and LP 877-72 to be $-1.00 \pm 0.35 \times 10^{44}$ and $-5.21 \pm 0.12 \times 10^{43}$ erg, respectively. We have also shown that both the systems are stable enough to survive longer than ∼10 Gyr.

(vii) We have discussed the possibility of hosting exoplanets on each of the components of the VLM binaries. We should expect to find up to 'two' exoplanets around LP 877-72 B, whereas the maximum probability for hosting exoplanets for LP 877-72 A, LP 1033-31 A, and LP 1033-31 B is estimated to be ∼50 per cent.

In future, the follow-up spectroscopic observations of the detected individual components for both LP 1033-31 and LP 877-72 can be made with AO. This would be very useful for further understanding of the onset of dust cloud formation in their atmosphere. The detection and characterization of the two VLM binaries including an equal mass binary give us the opportunity to constrain the evolutionary models as well as to perform the follow-up RV observations for the possible detection of the exoplanets around them.

ACKNOWLEDGEMENTS

We thank the anonymous referee for a rigorous review that greatly improved the manuscript. SK and AR are especially grateful to Sachindra Naik and Mudit Kumar Srivastava from *Physical Research Laboratory* (PRL) for their valuable inputs and discussion. The research leading to these results has received funding from the French 'Programme National de Physique Stellaire' and the Programme National de Planetologie of CNRS (INSU). The computations were performed at the *Pôle Scientifique de Modélisation Numérique* (PSMN) at the *École Normale Supérieure* (ENS) in Lyon, and at the *Gesellschaft für Wissenschaftliche Datenverarbeitung Göttingen* in collaboration with the Institut für Astrophysik Göttingen. DH was supported by the Collaborative Research Centre SFB 881 'The Milky Way System' (subproject A4) of the German Research Foundation (DFG).

This research is based on the observations obtained with the NaCo instrument on the VLT@ESO telescope at Paranal Observatory under programme ID 091.C-0501(B).

DATA AVAILABILITY

The data underlying this article are available in the ESO archive (https://archive.eso.org/eso/eso_archive_main.html).

REFERENCES

Allen P. R., Burgasser A. J., Faherty J. K., Kirkpatrick J. D., 2012, AJ, 144, 62
Anders F. et al., 2019, A&A, 628, A94
Anglada-Escudé G. et al., 2016, Nature, 536, 437
Apps K. et al., 2010, PASP, 122, 156
Bailer-Jones C. A. L., Rybizki J., Fouesneau M., Mantelet G., Andrae R., 2018, AJ, 156, 58
Baraffe I., Chabrier G., Allard F., Hauschildt P. H., 1998, A&A, 337, 403
Baraffe I., Homeier D., Allard F., Chabrier G., 2015, A&A, 577, A42
Baron F. et al., 2015, ApJ, 802, 37
Basri G., Reiners A., 2006, AJ, 132, 663
Bate M. R., 2009, MNRAS, 397, 232
Bate M. R., 2012, MNRAS, 419, 3115
Bate M. R., Bonnell I. A., Bromm V., 2003, MNRAS, 339, 577
Benedict G. F. et al., 2016, AJ, 152, 141
Bergfors C. et al., 2010, A&A, 520, A54
Beuzit J. L. et al., 2004, A&A, 425, 997
Billères M., Delfosse X., Beuzit J.-L., Forveille T., Marchal L., Martín E. L., 2005, A&A, 440, L55
Bochanski J. J., Hawley S. L., Covey K. R., West A. A., Reid I. N., Golimowski D. A., Ivezić Ž., 2010, AJ, 139, 2679
Bonfils X. et al., 2012, A&A, 546, A27
Bonfini P., Hatzidimitriou D., Pietsch W., Reig P., 2009, A&A, 507, 705
Boss A. P., 2001, ApJ, 551, L167
Bouy H., Brandner W., Martín E. L., Delfosse X., Allard F., Basri G., 2003, AJ, 126, 1526
Bouy H. et al., 2004, A&A, 423, 341
Boyajian T. S. et al., 2012, ApJ, 757, 112
Boyd M. R., Winters J. G., Henry T. J., Jao W.-C., Finch C. T., Subasavage J. P., Hambly N. C., 2011, AJ, 142, 10
Burgasser A. J., Kirkpatrick J. D., Reid I. N., Brown M. E., Miskey C. L., Gizis J. E., 2003, ApJ, 586, 512
Burgasser A. J., Reid I. N., Siegler N., Close L., Allen P., Lowrance P., Gizis J., 2007a, in Reipurth B., Jewitt D., Keil K., eds, Protostars and Planets V. University of Arizona Press, Tucson, p. 427
Burgasser A. J., Looper D. L., Kirkpatrick J. D., Liu M. C., 2007b, ApJ, 658, 557
Burningham B. et al., 2010, MNRAS, 404, 1952
Caballero J. A., 2007a, A&A, 462, L61
Caballero J. A., 2007b, ApJ, 667, 520
Caballero J. A., 2009, A&A, 507, 251
Caballero J. A., Martín E. L., Dobbie P. D., Barrado Y Navascués D., 2006, A&A, 460, 635
Caloi V., Cardini D., D'Antona F., Badiali M., Emanuele A., Mazzitelli I., 1999, A&A, 351, 925
Chabrier G., Baraffe I., 1997, A&A, 327, 1039
Chabrier G., Baraffe I., Allard F., Hauschildt P., 2000, ApJ, 542, 464
Chabrier G., Johansen A., Janson M., Rafikov R., 2014, in Beuther H., Klessen R. S., Dullemond C. P., Henning T., eds, Protostars and Planets VI. University of Arizona Press, Tucson, p. 619
Chauvin G., Lagrange A.-M., Dumas C., Zuckerman B., Mouillet D., Song I., Beuzit J.-L., Lowrance P., 2004, A&A, 425, L29
Close L. M., Siegler N., Freed M., Biller B., 2003, ApJ, 587, 407
Close L. M. et al., 2007, ApJ, 660, 1492
Cloutier R., 2019, AJ, 158, 81
Cortés-Contreras M. et al., 2017, A&A, 597, A47
Couteau P., 1960, J. Observateurs, 43, 41
Cruz K. L., Reid I. N., Liebert J., Kirkpatrick J. D., Lowrance P. J., 2003, AJ, 126, 2421
Cutri R. M. et al., 2003, 2MASS All-Sky Catalog of Point Sources, VizieR Online Data Catalog, 2246
Dahn C. C. et al., 2002, AJ, 124, 1170
De Rosa R. J. et al., 2014, MNRAS, 437, 1216
Deacon N. R. et al., 2014, ApJ, 792, 119
Delfosse X., Forveille T., Ségransan D., Beuzit J.-L., Udry S., Perrier C., Mayor M., 2000, A&A, 364, 217
Dhital S., West A. A., Stassun K. G., Bochanski J. J., 2010, AJ, 139, 2566
Dieterich S. B., Henry T. J., Golimowski D. A., Krist J. E., Tanner A. M., 2012, AJ, 144, 64
Duchêne G., Kraus A., 2013, ARA&A, 51, 269
Dupuy T. J., Liu M. C., 2017, ApJS, 231, 15
Duquennoy A., Mayor M., 1991, A&A, 500, 337
El-Badry K., Rix H.-W., Tian H., Duchêne G., Moe M., 2019, MNRAS, 489, 5822
Faherty J. K., Burgasser A. J., West A. A., Bochanski J. J., Cruz K. L., Shara M. M., Walter F. M., 2010, AJ, 139, 176
Finch C. T., Zacharias N., Subasavage J. P., Henry T. J., Riedel A. R., 2014, AJ, 148, 119
Fischer D. A., Marcy G. W., 1992, ApJ, 396, 178
Frith J. et al., 2013, MNRAS, 435, 2161
Gaia Collaboration, 2018, A&A, 616, A1
Gaidos E. et al., 2014, MNRAS, 443, 2561
Gálvez-Ortiz M. C., Solano E., Lodieu N., Aberasturi M., 2017, MNRAS, 466, 2983
Giclas H. L., Burnham R., Thomas N. G., 1971, Lowell proper motion survey Northern Hemisphere. The G numbered stars. 8991 stars fainter than magnitude 8 with motions 0".26/year, Lowell Observatory, Flagstaff, Arizona
Giclas H. L., Burnham R. J., Thomas N. G., 1978, Lowell Obs. Bull., 8, 89
Gillon M. et al., 2017, Nature, 542, 456
Gizis J. E., Reid I. N., Knapp G. R., Liebert J., Kirkpatrick J. D., Koerner D. W., Burgasser A. J., 2003, AJ, 125, 3302
Goldman B., Marsat S., Henning T., Clemens C., Greiner J., 2010, MNRAS, 405, 1140
Golimowski D. A. et al., 2004, AJ, 128, 1733
Gullikson K., Kraus A., Dodson-Robinson S., 2016, AJ, 152, 40
Halbwachs J. L., Mayor M., Udry S., Arenou F., 2003, A&A, 397, 159
Hardegree-Ullman K. K., Cushing M. C., Muirhead P. S., Christiansen J. L., 2019, AJ, 158, 75
Hawley S. L. et al., 2002, AJ, 123, 3409
Henry T. J., McCarthy Donald W. J., 1993, AJ, 106, 773
Henry T. J., Ianna P. A., Kirkpatrick J. D., Jahreiss H., 1997, AJ, 114, 388
Henry T. J., Franz O. G., Wasserman L. H., Benedict G. F., Shelus P. J., Ianna P. A., Kirkpatrick J. D., McCarthy Donald W. J., 1999, ApJ, 512, 864
Irwin J. M., Berta-Thompson Z. K., Charbonneau D., Dittmann J., Falco E. E., Newton E. R., Nutzman P., 2015, in Proc. Conf., 18th Cambridge Workshop on Cool Stars, Stellar Systems, and the Sun. Lowell Observatory, Flagstaff, Arizona, p. 767
Janson M. et al., 2012, ApJ, 754, 44
Janson M., Bergfors C., Brandner W., Kudryavtseva N., Hormuth F., Hippler S., Henning T., 2014, ApJ, 789, 102
Joergens V., 2006, A&A, 446, 1165
Karmakar S. et al., 2016, MNRAS, 459, 3112
Karmakar S., Pandey J. C., Airapetian V. S., Misra K., 2017, ApJ, 840, 102
Kesseli A. Y., West A. A., Veyette M., Harrison B., Feldman D., Bochanski J. J., 2017, ApJS, 230, 16
Kirkpatrick J. D. et al., 2014, ApJ, 783, 122
Kirkpatrick J. D. et al., 2016, ApJS, 224, 36
Konopacky Q. M., Ghez A. M., Rice E. L., Duchêne G., 2007, ApJ, 663, 394
Konopacky Q. M., Ghez A. M., Barman T. S., Rice E. L., Bailey J. I. I., White R. J., McLean I. S., Duchêne G., 2010, ApJ, 711, 1087
Kraus A. L., Hillenbrand L. A., 2007, ApJ, 664, 1167
Kraus A. L., Hillenbrand L. A., 2009, ApJ, 703, 1511
Kraus A. L., Ireland M. J., Hillenbrand L. A., Martinache F., 2012, ApJ, 745, 19
Kraus A. L., Ireland M. J., Huber D., Mann A. W., Dupuy T. J., 2016, AJ, 152, 8
Krumholz M. R., Myers A. T., Klein R. I., McKee C. F., 2016, MNRAS, 460, 3272
Kurtev R. et al., 2017, MNRAS, 464, 1247
Lada C. J., 2006, ApJ, 640, L63
Lafrenière D., Jayawardhana R., Janson M., Helling C., Witte S., Hauschildt P., 2011, ApJ, 730, 42
Lane B. F., Boden A. F., Kulkarni S. R., 2001, ApJ, 551, L81

Law N. M., Hodgkin S. T., Mackay C. D., 2006, MNRAS, 368, 1917
Law N. M., Dhital S., Kraus A., Stassun K. G., West A. A., 2010, ApJ, 720, 1727
Lenzen R. et al., 2003, in Iye M., Moorwood A. F. M., eds, Proc. SPIE Conf. Ser., Vol. 4841, Instrument Design and Performance for Optical/Infrared Ground-based Telescopes. SPIE, Bellingham, p. 944
Lépine S., 2008, AJ, 135, 2177
Lépine S., Gaidos E., 2011, AJ, 142, 138
Lépine S., Gaidos E., 2013, Astron. Nachr., 334, 176
Lépine S., Shara M. M., 2005, AJ, 129, 1483
Lépine S., Hilton E. J., Mann A. W., Wilde M., Rojas-Ayala B., Cruz K. L., Gaidos E., 2013, AJ, 145, 102
Luhman K. L., 2004, ApJ, 614, 398
Luhman K. L., 2012, ARA&A, 50, 65
Luhman K. L., 2014, ApJ, 781, 4
Luhman K. L., Joergens V., Lada C., Muzerolle J., Pascucci I., White R., 2007, in Reipurth B., Jewitt D., Keil K., eds, Protostars and Planets V. University of Arizona Press, Tucson, p. 443
Luhman K. L., Mamajek E. E., Allen P. R., Muench A. A., Finkbeiner D. P., 2009, ApJ, 691, 1265
Luyten W. J., 1979a, LHS catalogue. A catalogue of stars with proper motions exceeding 0”5 annually, University of Minnesota, Minneapolis
Luyten W. J., 1979b, New Luyten catalogue of stars with proper motions larger than two tenths of an arcsecond, University of Minnesota, Minneapolis
Luyten W. J., 1980, NLTT Catalogue. Volume_III. 0_-to -30_-, University of Minnesota, Mineapolis, Minnesota, USA
Luyten W. J., 1995, VizieR Online Data Catalog: NLTT Catalogue (Luyten, 1979), VizieR Online Data Catalog, p. I/98A
Matson R. A., Howell S. B., Horch E. P., Everett M. E., 2018, AJ, 156, 31
Moe M., Di Stefano R., 2017, ApJS, 230, 15
Moe M., Kratter K. M., 2019, preprint (arXiv:1912.01699)
Muirhead P. S., Dressing C. D., Mann A. W., Rojas-Ayala B., Lépine S., Paegert M., De Lee N., Oelkers R., 2018, AJ, 155, 180
Murphy S. J., Moe M., Kurtz D. W., Bedding T. R., Shibahashi H., Boffin H. M. J., 2018, MNRAS, 474, 4322
Mužić K. et al., 2012, AJ, 144, 180
Myers A. T., Klein R. I., Krumholz M. R., McKee C. F., 2014, MNRAS, 439, 3420
Nakajima T., Oppenheimer B. R., Kulkarni S. R., Golimowski D. A., Matthews K., Durrance S. T., 1995, Nature, 378, 463
Ngo H. et al., 2016, ApJ, 827, 8
Offner S. S. R., Klein R. I., McKee C. F., Krumholz M. R., 2009, ApJ, 703, 131
Padoan P., Nordlund Å., 2004, ApJ, 617, 559
Pandey J. C., Karmakar S., 2015, AJ, 149, 47
Phan-Bao N., Martín E. L., Reylé C., Forveille T., Lim J., 2005, A&A, 439, L19
Pokorny R. S., Jones H. R. A., Hambly N. C., 2003, A&A, 397, 575
Radigan J., Lafrenière D., Jayawardhana R., Doyon R., 2008, ApJ, 689, 471
Radigan J., Lafrenière D., Jayawardhana R., Doyon R., 2009, ApJ, 698, 405
Raghavan D. et al., 2010, ApJS, 190, 1
Rajpurohit A. S., Reylé C., Allard F., Homeier D., Schultheis M., Bessell M. S., Robin A. C., 2013, A&A, 556, A15
Rebolo R., Zapatero Osorio M. R., Martín E. L., 1995, Nature, 377, 129
Reid I. N., Gizis J. E., 1997, AJ, 114, 1992
Reid I. N., Gizis J. E., Kirkpatrick J. D., Koerner D. W., 2001, AJ, 121, 489
Reid I. N., Cruz K. L., Allen P. R., 2007, AJ, 133, 2825
Reiners A. et al., 2018, A&A, 612, A49
Reipurth B., Clarke C., 2001, AJ, 122, 432
Reylé C., Robin A. C., 2004, A&A, 421, 643
Reylé C., Scholz R.-D., Schultheis M., Robin A. C., Irwin M., 2006, MNRAS, 373, 705
Riaz R., Vanaverbeke S., Schleicher D. R. G., 2018, MNRAS, 478, 5460
Ross F. E., 1939, AJ, 48, 163
Rousset G. et al., 2003, in Wizinowich P. L., Bonaccini D., eds, Proc. SPIE Conf. Ser., Vol. 4839, Adaptive Optical System Technologies II. SPIE, Bellingham, p. 140
Salim S., Gould A., 2003, ApJ, 582, 1011
Sana H. et al., 2012, Science, 337, 444
Savanov I. S. et al., 2016, AcA, 66, 381
Schneider A. C., Greco J., Cushing M. C., Kirkpatrick J. D., Mainzer A., Gelino C. R., Fajardo-Acosta S. B., Bauer J., 2016, ApJ, 817, 112
Scholz R.-D., Meusinger H., Jahreiß H., 2005, A&A, 442, 211
Ségransan D., Delfosse X., Forveille T., Beuzit J. L., Udry S., Perrier C., Mayor M., 2000, A&A, 364, 665
Ségransan D., Kervella P., Forveille T., Queloz D., 2003, A&A, 397, L5
Shatsky N., Tokovinin A., 2002, A&A, 382, 92
Siegler N., Close L. M., Cruz K. L., Martín E. L., Reid I. N., 2005, ApJ, 621, 1023
Skrutskie M. F. et al., 2006, AJ, 131, 1163
Smith L., Lucas P. W., Burningham B., Jones H. R. A., Smart R. L., Andrei A. H., Catalán S., Pinfield D. J., 2014, MNRAS, 437, 3603
Stamatellos D., Whitworth A. P., 2009, MNRAS, 392, 413
Stassun K. G. et al., 2018, AJ, 156, 102
Stassun K. G. et al., 2019, AJ, 158, 138
Stetson P. B., 1987, PASP, 99, 191
Stetson P. B., 1990, PASP, 102, 932
Tody D., 1986, The IRAF Data Reduction and Analysis System, Instrumentation in astronomy VI, Vol. 627, Society of Photo-Optical Instrumentation Engineers, Bellingham, Washington USA, p. 733
Tody D., 1993, Astronomical Data Analysis Software and Systems II, Vol. 52, Astronomical Society of the Pacific Conference Series, San Francisco, U.S, p. 173
Tuomi M. et al., 2019, preprint (arXiv:1906.04644)
Umbreit S., Burkert A., Henning T., Mikkola S., Spurzem R., 2005, ApJ, 623, 940
van Maanen A., 1915, PASP, 27, 240
Wang J., Fischer D. A., Xie J.-W., Ciardi D. R., 2014, ApJ, 791, 111
Wang J., Fischer D. A., Horch E. P., Xie J.-W., 2015a, ApJ, 806, 248
Wang J., Fischer D. A., Xie J.-W., Ciardi D. R., 2015b, ApJ, 813, 130
Ward-Duong K. et al., 2015, MNRAS, 449, 2618
Weinberg M. D., Shapiro S. L., Wasserman I., 1987, ApJ, 312, 367
West A. A., Hawley S. L., Bochanski J. J., Covey K. R., Reid I. N., Dhital S., Hilton E. J., Masuda M., 2008, AJ, 135, 785
Whitworth A. P., Zinnecker H., 2004, A&A, 427, 299
Whitworth A., Bate M. R., Nordlund Å., Reipurth B., Zinnecker H., 2007, in Reipurth B., Jewitt D., Keil K., eds, Protostars and Planets V. University of Arizona Press, Tucson, p. 459
Winters J. G. et al., 2015, AJ, 149, 5
Winters J. G. et al., 2019a, AJ, 157, 216
Winters J. G. et al., 2019b, AJ, 158, 152
Wolf M., 1919, Veroeffentlichungen der Badischen Sternwarte zu Heidelberg, 10, 195
Wright E. L. et al., 2010, AJ, 140, 1868
Wroblewski H., Torres C., 1995, A&AS, 110, 27
York D. G. et al., 2000, AJ, 120, 1579
Zboril M., Byrne P. B., Rolleston W. R. J. R., 1997, MNRAS, 284, 685
Ziegler C., Tokovinin A., Briceño C., Mang J., Law N., Mann A. W., 2020, AJ, 159, 19
Zuckerman B., Song I., 2009, A&A, 493, 1149

This paper has been typeset from a TEX/LATEX file prepared by the author.